AIAA JOURNAL
Vol. 38, No. 2, February 2000

Determination of Nonideal Beam Boundary Conditions: A Spectral Element Approach

Usik Lee* and Joohong Kim†
Inha University, Inchon 402-751, Republic of Korea

A spectral element approach to determine the nonideal or unknown structural boundary conditions of beams is introduced. The nonideal structural boundary conditions are represented by the frequency-dependent effective boundary springs: transverse springs and rotational springs. The effective boundary spring constants are then determined from the measured frequency response functions in conjunction with the spectral element method. Experiments are conducted for the one-end-supported and the two-end-supported beams to verify the present approach of boundary conditions identification. The analytical predictions obtained by using the identified boundary conditions are very close to the experiment measurements.

Nomenclature

$\boldsymbol{A}_{\rm bm}$, etc.	= submatrices defined in Eqs. (16) and (25)
a_i	= nodal transverse inertance (at the ith node)
$\boldsymbol{D}, \boldsymbol{D}_m, \boldsymbol{D}_u$	= nodal inertances vectors
EI	= beam bending stiffness
$\boldsymbol{F}, \boldsymbol{F}_b, \boldsymbol{F}_e$	= nodal forces vectors
$\boldsymbol{f}, \boldsymbol{f}_b, \boldsymbol{f}_e$	= nodal forces vectors multiplied by $-\omega^2/P$
$g_i(x)$	= exact shape functions
k	= wave number
K_v, K_ϕ	= transverse and rotational spring constants
L	= length of finite beam element
M, M_1, M_2	= resultant bending moments
p, P	= applied point load
Q, Q_1, Q_2	= resultant transverse shear forces
$\boldsymbol{s}$, s_{ij}	= spectral element matrix
$\boldsymbol{U}_m, \boldsymbol{U}_u$	= nodal degree of freedom (DOF) vectors
$v(x, t)$	= transverse beam deflection
α_i	= nodal rotational inertance (at the ith node)
ξ	= function defined in Eq. (10)
ρA	= mass per unit length of beam
ϕ_i	= nodal rotational angle (at the ith node)
ω	= circular frequency

Subscripts

b	= quantities related to (unknown) boundary forces vector
e	= quantities related to (known) external forces vector
m	= quantities related to measured (or known) DOF
u	= quantities related to unmeasured (or unknown) DOF
1, 2, . . . , 6	= node numbers

Superscripts

1, 2, 3	= spectral element number
ˆ	= spectral components

I. Introduction

STRUCTURAL identification, model updating, and health monitoring have been intense research activities during the last decade.[1–3] The identification of a structural system has the primary objective of deriving a mathematical model that reproduces the observed behavior of that structure. Because of the increasing complexity of modern structures, an accurate mathematical model has become a necessity for successful design of mechanical systems. However, one often experiences the problem that a mathematical model [e.g., finite element method (FEM) model] does not predict the dynamic behavior of a real structure very well when compared with the measurements. The discrepancy may be caused by the inaccurate identification of the structural parameters such as the mass, stiffness, and damping matrices of the FEM model. This is why there have been intense efforts to determine accurate structural parameters in the subject of structural system identification.

Dynamic characteristics of a structure certainly depend on its structural boundary conditions. Thus, the structural boundary conditions should be considered as the additional structural parameter and should be identified accurately before structural dynamics analysis. It is very often to simplify the real (nonideal) structural boundary conditions as the ideal ones such as the perfectly clamped boundary condition and the perfectly simply supported boundary condition. Unfortunately, the practical structural boundary conditions are not so ideal: they are mostly nonideal or unknown in nature. Thus, simplifying the nonideal structural boundary conditions as the ideal ones is certainly one of the important error sources between the measurement and the analytical prediction.

Despite the importance of the structural boundary conditions identification, there have been relatively few efforts to identify the nonideal structural boundary conditions when compared to the efforts given to the identifications of structural parameters and damages. In the literature Wang and Chen[4] is likely to be one of few recent works in the identification of nonideal structural boundary conditions. They represented the unknown boundaries of a slender beam as the additional stiffness matrix (called as the boundary stiffness matrix) in their FEM. The boundary stiffness matrix was determined from the measured structure modal parameters (i.e., natural frequencies and mode vectors).

As mentioned, Wang and Chen[4] used the FEM of a beam and the measured structure modal parameters in their approach (i.e., FEM-modal parameters approach). The FEMs usually provide less accurate structural dynamic characteristics, especially at high frequencies. It is not an easy task even today to extract accurate modal parameters from experiments. Thus, instead of the FEM-modal parameter approach, a new more reliable and easy-to-use approach is desirable.

In contrast to FEM, the spectral element method (SEM) is well recognized to provide very accurate dynamic characteristics of a structure even at high frequency.[5] The spectral element matrix used in SEM is the same as the exact dynamic stiffness matrix in nature and was used by Lee and his colleagues[6–10] to solve structural dynamics problems and Doyle and his colleagues[11,12] to investigate

Received 20 August 1998; presented as Paper 99-1311 at the AIAA/ASME/ASCE/AHS/ASC 40th Structures, Structural Dynamics, and Materials Conference, St. Louis, MO, 12–15 April 1999; revision received 25 May 1999; accepted for publication 17 June 1999.

*Professor, Department of Mechanical Engineering, 253 Yonghyun-Dong, Nam-Ku. Senior Member AIAA.

†Graduate Research Assistant, Department of Mechanical Engineering, 253 Yonghyun-Dong, Nam-Ku.

the wave propagation in structures. The spectral element matrix is exact in the sense that it is formulated from the exact shape functions (or wave modes), which treat the mass distribution exactly. Spectral elements can be assembled in a completely analogous way to that used for FEM. In SEM all calculations are conducted in frequency domain by using the fast Fourier transform (FFT) algorithm.[13] To obtain the time-domain solutions, the inverse FFT (IFFT) algorithm is then used. The FFT and IFFT algorithms-based spectral analysis approach combined with the main features of FEM has been called the SEM in the literature.[5–11] In SEM the general solution is assumed in the spectral form and a sufficient number of spectral components can be efficiently computed and summed by using FFT and IFFT algorithms. This solution approach has been found to improve the solution accuracy significantly, especially at high frequency, while consuming less computational time when compared with FEM approach.[9]

Because of the apparent advantages of SEM, it seems to be reasonable to use the SEM, instead of the FEM, to improve the identification of nonideal structural boundary. Because it is not always easy to extract accurate modal parameters from experiments, it seems to be more convenient to determine the nonideal boundary conditions directly from measured frequency response functions (FRF), instead of modal parameters. Hence, this paper introduces a new approach based on the spectral element beam model and the measured FRF, i.e., the SEM-FRF approach.

II. Spectral Beam Element Model

The more accurate structure model of a beam structure will provide more accurate identification of the beam boundary conditions. In this paper, the Bernoulli–Euler beam model is adopted just for simplicity. Extension of this paper to include the transverse shear, rotary inertia, axial modes, and out-of-plane bending modes effects in the simple beam model should be in due course.

To apply the spectral element analysis approach to the Bernoulli–Euler beam model, the spectral element should be formulated first. In general, the spectral element formulation begins with the equations of motion of a structure without neglecting inertia. For a finite Bernoulli–Euler beam element of length L, the equation of motion is given by

$$EI\frac{\partial^4 v}{\partial x^4} + \rho A\frac{\partial^2 v}{\partial t^2} = p(x,t) \tag{1}$$

Assume that the applied load and the beam response have the spectral representations

$$v(x,t) = \sum_{\omega=-\infty}^{\infty} \hat{v}(x)e^{i\omega t}, \qquad p(x,t) = \sum_{\omega=-\infty}^{\infty} \hat{p}(x)e^{i\omega t} \tag{2}$$

The spectral components are spatially dependent Fourier coefficients, and thus they are functions of circular frequency ω. For shorthand, the summation and the superscript used for spectral representations will be removed in the following without causing confusions.

For the finite beam element with the nodal degrees of freedom (DOF) specified at its two end nodes 1 and 2, the spectral component of transverse deflection can be derived in the form of

$$v(x) = g_1(x)v_1 + g_2(x)\phi_1 + g_3(x)v_2 + g_4(x)\phi_2 \tag{3}$$

where v_i and ϕ_i represent the transverse nodal DOF and the rotational nodal DOF, respectively, and the frequency dependent exact shape functions $g_i(x)$ can be found in Ref. 5.

The relationships for the structural quantities are given by

$$M = EI\frac{\mathrm{d}^2 v}{\mathrm{d}x^2}, \qquad Q = -EI\frac{\mathrm{d}^3 v}{\mathrm{d}x^3} \tag{4}$$

The nodal forces and moments at node 1 (i.e., $x=0$) and node 2 (i.e., $x=L$) can be written as

$$Q_1 = -Q(0), \qquad Q_2 = -Q(L)$$
$$M_1 = -M(0), \qquad M_2 = -M(L) \tag{5}$$

Thus, the relationships between the nodal forces/moments and the nodal DOF can be derived in the form of

$$\begin{Bmatrix} Q_1 \\ M_1 \\ Q_2 \\ M_2 \end{Bmatrix} = \begin{bmatrix} s_{11} & s_{12} & s_{13} & s_{14} \\ & s_{22} & s_{23} & s_{24} \\ & & s_{33} & s_{34} \\ & \text{symmetric} & & s_{44} \end{bmatrix} \begin{Bmatrix} v_1 \\ \phi_1 \\ v_2 \\ \phi_2 \end{Bmatrix} \quad \text{or} \quad \boldsymbol{f} = \boldsymbol{su} \tag{6}$$

where $\boldsymbol{s}$ is the spectral element matrix and, in SEM, the corresponding finite beam element is called the spectral element. The components of spectral element matrix are given by

$$s_{11} = \xi(\sin kL\cosh kL + \cos kL\sinh kL)(kL)^3$$
$$s_{12} = \xi\sin kL\sinh kL(kL)^2 L$$
$$s_{13} = -\xi(\sin kL + \sinh kL)(kL)^3$$
$$s_{14} = \xi(\cosh kL - \cos kL)(kL)^2 L$$
$$s_{22} = \xi(\sin kL\cos kL - \cos kL\sinh kL)kL^3$$
$$s_{23} = \xi(\cos kL - \cosh kL)(kL)^2 L$$
$$s_{24} = \xi(\sinh kL - \sin kL)kL^3$$
$$s_{33} = \xi(\sin kL\cosh kL + \cos kL\sin kL)(kL)^3$$
$$s_{34} = -\xi\sin kL\sinh kL(kL)^2 L$$
$$s_{44} = \xi(\sin kL\cosh kL - \cos kL\sinh kL)kL^3$$
$$\xi = (EI)/(L^3 z_0) \tag{7}$$

In Eq. (7), k is the wave number, and it is related to ω through the spectrum relation as

$$k^4 = \omega^2\rho A/EI \tag{8}$$

As far as a finite straight beam is uniform without any sources of discontinuity, it can be represented by a single spectral element regardless of its length. In contrast to the conventional finite element, this single spectral element still provides very accurate solutions.[5] However, if there exist sources of discontinuity such as the point loads acting on a uniform beam, the beam should be spatially discretized into several spectral elements. All spectral elements can be assembled to form a global structure system in a completely analogous way to that used for FEM.

Figure 1 shows a beam with a point load $p(t)$ at $x=a$. The beam is discretized into two spectral elements so that the point load is located at the junction of two elements. The point load $p(t)$ is Fourier transformed to obtain $P(\omega)$ by using the FFT algorithm. Assembling two spectral elements gives the following global spectral matrix equation:

$$\begin{bmatrix} s_{11}^1 & s_{12}^1 & s_{13}^1 & s_{14}^1 & 0 & 0 \\ s_{21}^1 & s_{22}^1 & s_{22}^1 & s_{24}^1 & 0 & 0 \\ s_{31}^1 & s_{32}^1 & s_{33}^1 + s_{11}^2 & s_{34}^1 + s_{12}^2 & s_{13}^2 & s_{14}^2 \\ s_{41}^1 & s_{42}^1 & s_{43}^1 + s_{21}^2 & s_{44}^1 + s_{22}^2 & s_{23}^2 & s_{24}^2 \\ 0 & 0 & s_{31}^2 & s_{32}^2 & s_{33}^2 & s_{34}^2 \\ 0 & 0 & s_{41}^2 & s_{42}^2 & s_{43}^2 & s_{44}^2 \end{bmatrix} \begin{Bmatrix} v_1 \\ \phi_1 \\ v_2 \\ \phi_2 \\ v_3 \\ \phi_3 \end{Bmatrix} = \begin{Bmatrix} 0 \\ 0 \\ P(\omega) \\ 0 \\ 0 \\ 0 \end{Bmatrix} \tag{9}$$

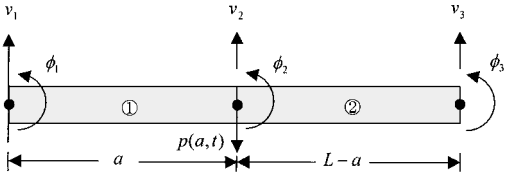

Fig. 1 Spectral element discretization of a beam subjected to a point load $p(a,t)$.

Table 1 Comparison of the natural frequencies of a simply supported square plate[8]

Mode	Frequency, Hz: Exact solution	SEM, 1 element	FEM, 14 × 14 elements
1st (1, 1)	6.21	6.21	6.2
2nd (1, 2)	15.53	15.53	15.12
3rd (2, 2)	24.86	24.86	23.75
5th (2, 3)	40.39	40.38	38.12
10th (4, 4)	99.42	99.43	95.18
15th (5, 5)	155.35	155.35	141.37
20th (5, 6)	189.53	189.53	171.48

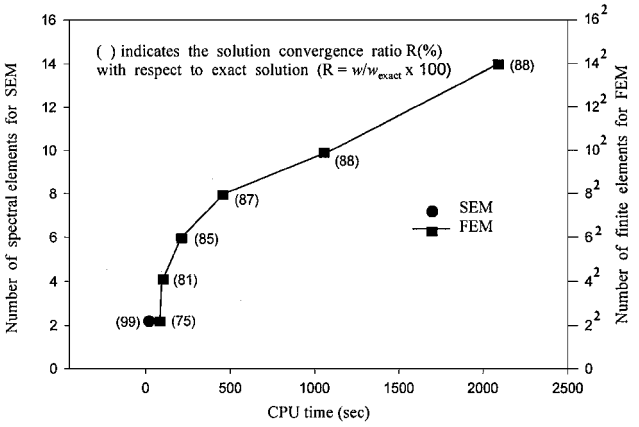

Fig. 2 Comparison of the solution convergence ratio ($R = w/w_{exact}$) for SEM and FEM with respect to CPU time.[8]

or, simply,

$$\boldsymbol{SU} = \boldsymbol{F} \tag{10}$$

In Eq. (9) the superscript indicates each spectral element, and the subscript indicates each component of the corresponding spectral element matrix given in Eq. (6). In Eq. (10) $\boldsymbol{U}$ is the frequency-dependent nodal DOF vector, and it can be readily obtained analogous to the static problem. The IFFT algorithm is then used to obtain the time-domain response efficiently.

The high-solution accuracy and computational efficiency of SEM has been well proved for the vibrations of beams and plates in Refs. 8 and 10. For a simply supported rectangular plate subjected to an impulsive force at the midpoint, Fig. 2 from Ref. 8 shows that SEM requires much less CPU time to obtain the same level of solution accuracy as achieved by FEM. Table 1 from Ref. 8 also shows that the natural frequencies obtained by using just one spectral element are almost identical to the exact natural frequencies, whereas those obtained by using a sufficient number of conventional finite elements are not so accurate, especially at high vibration modes.

III. Determination of Nonideal Boundary Conditions

Nonideal (or unknown) boundary conditions of a beam structure can be represented as the frequency-dependent effective boundary springs at its boundaries: the transverse spring K_v and the rotational spring K_ϕ. When both effective boundary spring constants are infinite at a boundary, the boundary is recognized as the perfectly clamped boundary, whereas they are zeros as the perfectly free boundary, for instance. Thus, any nonideal beam boundary can be represented by simply determining the values of effective boundary spring constants.

This section introduces a methodology to determine the effective boundary spring constants by utilizing the measured FRF. Two simple beams with representative boundary conditions are considered in this paper: one-end-supported (or cantilever-type) beam and two-end-supported beam. Figure 3 shows the general procedure to identify the nonideal boundary condition by using the MATLAB® program ID-BC developed in this study.

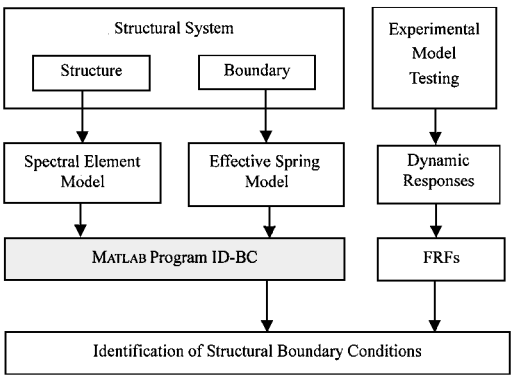

Fig. 3 Procedure for the identification of structural boundary conditions.

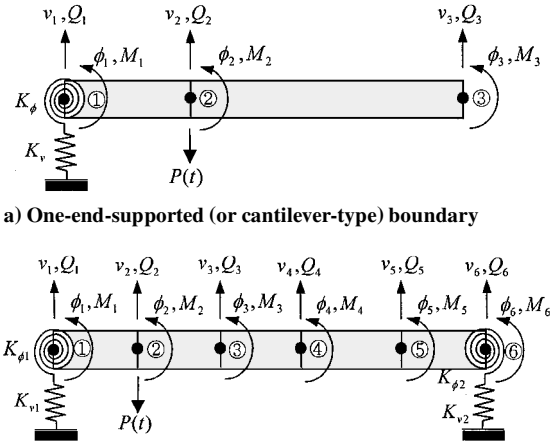

a) One-end-supported (or cantilever-type) boundary

b) Two-end-supported (or clamped) boundary

Fig. 4 Modeling of the nonideal structural boundary conditions.

A. One-End-Supported Boundary

Consider a one-end-supported (or cantilever-type) beam of Fig. 4a. The beam is discretized into two spectral elements so that the applied load is located at node 2. The nonideal boundary at node 1 is represented by two (unknown) effective boundary springs: a transverse spring K_v and a rotational spring K_ϕ. The global nodal DOF vector $\boldsymbol{U}$ can be divided into two nodal DOF vectors: the measured DOF vector $\boldsymbol{U}_m$ and the unmeasured DOF vector $\boldsymbol{U}_u$. As the transverse DOF, v_2 and v_3 at nodes 2 and 3 can be readily measured by experiments; they are considered as the measured DOF. However, v_1 and ϕ_1 at the boundary node 1 are not accessible to measure, ϕ_2 and ϕ_3 and are the rotational DOF relatively more delicate to measure when compared with measuring the transverse DOF. Thus, these four unmeasurable nodal DOF are considered as the unmeasured DOF. Thus, there are total six unknowns including four unmeasured DOF and two effective boundary spring constants.

Assembling two spectral elements of Fig. 4a, the (6 × 6) global spectral matrix equation is derived as

$$\begin{bmatrix} s_{11}^1 & s_{12}^1 & s_{13}^1 & s_{14}^1 & 0 & 0 \\ s_{21}^1 & s_{22}^1 & s_{22}^1 & s_{24}^1 & 0 & 0 \\ s_{31}^1 & s_{32}^1 & s_{33}^1 + s_{11}^2 & s_{34}^1 + s_{12}^2 & s_{13}^2 & s_{14}^2 \\ s_{41}^1 & s_{42}^1 & s_{43}^1 + s_{21}^2 & s_{44}^1 + s_{22}^2 & s_{23}^2 & s_{24}^2 \\ 0 & 0 & s_{31}^2 & s_{32}^2 & s_{33}^2 & s_{34}^2 \\ 0 & 0 & s_{41}^2 & s_{42}^2 & s_{43}^2 & s_{44}^2 \end{bmatrix} \begin{Bmatrix} v_1 \\ \phi_1 \\ v_2 \\ \phi_2 \\ v_3 \\ \phi_3 \end{Bmatrix} = \begin{Bmatrix} -K_v v_1 \\ -K_\phi \phi_1 \\ P \\ 0 \\ 0 \\ 0 \end{Bmatrix} \tag{11}$$

or, simply,

$$\boldsymbol{S}_{(6\times 6)}\boldsymbol{U} = \boldsymbol{F} \tag{12}$$

Dividing $\boldsymbol{U}$ into $\boldsymbol{U}_m$ (known, measured DOF) and $\boldsymbol{U}_u$ (unknown, unmeasured DOF), and also dividing $\boldsymbol{F}$ into $\boldsymbol{F}_b$ (unknown, boundary

forces vector) and $\boldsymbol{F}_e$ (known, external loads vector), Eq. (11) can be rewritten as

$$\begin{bmatrix} \boldsymbol{A}_{\mathrm{bm}} & \boldsymbol{A}_{\mathrm{bu}} \\ \boldsymbol{A}_{\mathrm{em}} & \boldsymbol{A}_{\mathrm{eu}} \end{bmatrix} \begin{Bmatrix} \boldsymbol{U}_m \\ \boldsymbol{U}_u \end{Bmatrix} = \begin{Bmatrix} \boldsymbol{F}_b \\ \boldsymbol{F}_e \end{Bmatrix} \tag{13}$$

where

$$\boldsymbol{U}_m = \{v_2 \quad v_3\}^T, \qquad \boldsymbol{U}_u = \{v_1 \quad \phi_1 \quad \phi_2 \quad \phi_3\}^T$$

$$\boldsymbol{F}_b = \{-K_v v_1 \quad -K_\phi \phi_1\}^T, \qquad \boldsymbol{F}_e = \{P \quad 0 \quad 0 \quad 0\}^T$$

$$\boldsymbol{A}_{\mathrm{bm}} = \begin{bmatrix} s^1_{13} & 0 \\ s^1_{23} & 0 \end{bmatrix}, \qquad \boldsymbol{A}_{\mathrm{bu}} = \begin{bmatrix} s^1_{11} & s^1_{12} & s^1_{14} & 0 \\ s^1_{21} & s^1_{22} & s^1_{24} & 0 \end{bmatrix}$$

$$\boldsymbol{A}_{\mathrm{em}} = \begin{bmatrix} s^1_{33} + s^2_{13} & s^2_{13} \\ s^1_{43} + s^2_{21} & s^2_{23} \\ s^2_{31} & s^2_{33} \\ s^2_{41} & s^2_{43} \end{bmatrix}, \qquad \boldsymbol{A}_{\mathrm{eu}} = \begin{bmatrix} s^1_{31} & s^1_{32} & s^1_{34} + s^2_{12} & s^2_{14} \\ s^1_{41} & s^1_{42} & s^1_{44} + s^2_{22} & s^2_{24} \\ 0 & 0 & s^2_{32} & s^2_{34} \\ 0 & 0 & s^2_{42} & s^2_{44} \end{bmatrix} \tag{14}$$

Because it is very convenient and customary for us to measure the vibration acceleration by simply using an accelerometer, the nodal displacements DOF of Eq. (13) will be represented in terms of the FRF parameters related to the nodal accelerations. The (transverse or rotational) inertance is a FRF parameter defined as the ratio of (transverse or rotational) acceleration to force.[14] Thus, replace the nodal displacements vector $\boldsymbol{U}$ with the corresponding nodal inertances vector $\boldsymbol{D}$ to rewrite Eq. (13) as

$$\begin{bmatrix} \boldsymbol{A}_{\mathrm{bm}} & \boldsymbol{A}_{\mathrm{bu}} \\ \boldsymbol{A}_{\mathrm{em}} & \boldsymbol{A}_{\mathrm{eu}} \end{bmatrix} \begin{Bmatrix} \boldsymbol{D}_m \\ \boldsymbol{D}_u \end{Bmatrix} = \begin{Bmatrix} \boldsymbol{f}_b \\ \boldsymbol{f}_e \end{Bmatrix} \tag{15}$$

where

$$\boldsymbol{D}_m = (-\omega^2/P)\boldsymbol{U}_m = \{a_2 \quad a_3\}^T$$

$$\boldsymbol{D}_u = (-\omega^2/P)\boldsymbol{U}_u = \{a_1 \quad \alpha_1 \quad \alpha_2 \quad \alpha_3\}^T$$

$$\boldsymbol{f}_b = (-\omega^2/P)\boldsymbol{F}_b = \{-K_v a_1 - K_\phi \alpha_1\}^T$$

$$\boldsymbol{f}_e = (-\omega^2/P)\boldsymbol{F}_e = \{-\omega^2 \quad 0 \quad 0 \quad 0\}^T \tag{16}$$

Unmeasured DOF vector $\boldsymbol{D}_u$ and the effective boundary spring constants K_v and K_ϕ can be readily obtained from Eq. (15) as follows. The effective boundary spring constants are first obtained from Eq. (16c) in terms of unknown boundary forces vector $\boldsymbol{f}_b$ as

$$\begin{Bmatrix} K_v \\ K_\phi \end{Bmatrix} = -\begin{bmatrix} 1/a_1 & 0 \\ 0 & 1/\alpha_1 \end{bmatrix} \boldsymbol{f}_b \tag{17}$$

The second row of Eq. (15) yields the unmeasured DOF vector $\boldsymbol{D}_u$ as

$$\boldsymbol{D}_u = \boldsymbol{A}_{\mathrm{eu}}^{-1}(\boldsymbol{f}_e - \boldsymbol{A}_{\mathrm{em}}\boldsymbol{D}_m) \tag{18}$$

Substituting Eq. (18) into the first row of Eq. (15) and eliminating $\boldsymbol{D}_u$ gives the unknown boundary forces vector $\boldsymbol{f}_b$ as

$$\boldsymbol{f}_b = (\boldsymbol{A}_{\mathrm{bm}} - \boldsymbol{A}_{\mathrm{bu}}\boldsymbol{A}_{\mathrm{eu}}^{-1}\boldsymbol{A}_{\mathrm{em}})\boldsymbol{D}_m + \boldsymbol{A}_{\mathrm{bu}}\boldsymbol{A}_{\mathrm{eu}}^{-1}\boldsymbol{f}_e \tag{19}$$

The effective spring constants are then obtained by substituting Eq. (19) into Eq. (17).

B. Two-End-Supported Boundary

As the second example, consider a two-end-supported beam of Fig. 4b. The nonideal boundary conditions at two end nodes (i.e., node 1 and node 6) are represented by four unknown effective boundary springs: two transverse springs K_{v1} and K_{v2} and two rotational springs $K_{\phi 1}$ and $K_{\phi 2}$. For the two spectral elements model there exist nine unmeasured DOF (i.e., four effective boundary springs, four unmeasured DOF at two end nodes, and one unmeasured DOF at loading point), whereas the dimension of the global spectral matrix equation (or number of equations) is six. Thus we need to obtain more equations to make a well-posed problem. Increasing the number of spectral elements by one increases the number of global nodal DOF by two, while the number of unmeasured DOF is increased by one (i.e., one rotational DOF). Hence, as shown in Fig. 4b, the beam is discretized into a total of five spectral elements so that the number of global nodal DOF and the dimension of global spectral matrix equation are now equal as 12. Among 12 global nodal DOF, v_2, v_3, v_4, and v_5 are the measured DOF and v_1, ϕ_1, ϕ_2, ϕ_3, ϕ_4, ϕ_5, and ϕ_6 are the unmeasured DOF. Thus, there are now a total of 12 unknowns including eight unmeasured DOF and four effective boundary spring constants. The four measured DOF, v_2, v_3, v_4, and v_5 are information enough to determine four effective boundary spring constants uniquely. It is not a hard business at all to obtain them experimentally for such a both-end-supported simple beam considered herein.

Assembling five spectral elements of Fig. 4b, we can obtain (12×12) global spectral matrix equation as

$$\boldsymbol{S}_{(12\times 12)}\boldsymbol{U} = \boldsymbol{F} \tag{20}$$

where

$$\boldsymbol{U} = \{v_1 \quad \phi_1 \quad v_2 \quad \phi_2 \quad v_3 \quad \phi_3 \quad v_4 \quad \phi_4 \quad v_5 \quad \phi_5 \quad v_6 \quad \phi_6\}^T$$

$$\boldsymbol{F} = \{-K_{v1}v_1 \quad -K_{\phi 1}\phi_1 \quad P \quad 0 \quad 0 \quad 0 \quad 0 \quad 0 \quad 0 \quad 0 \quad -K_{v2}v_6 \quad -K_{\phi 2}\phi_6\}^T \tag{21}$$

Similarly, as in the preceding section, Eq. (20) can be rewritten in terms of the measured DOF vector $\boldsymbol{U}_m$ and the unmeasured DOF vector $\boldsymbol{U}_u$ as

$$\begin{bmatrix} \boldsymbol{A}_{\mathrm{bm}} & \boldsymbol{A}_{\mathrm{bu}} \\ \boldsymbol{A}_{\mathrm{em}} & \boldsymbol{A}_{\mathrm{eu}} \end{bmatrix} \begin{Bmatrix} \boldsymbol{U}_m \\ \boldsymbol{U}_u \end{Bmatrix} = \begin{Bmatrix} \boldsymbol{F}_b \\ \boldsymbol{F}_e \end{Bmatrix} \tag{22}$$

where

$$\boldsymbol{U}_m = \{v_2 \quad v_3 \quad v_2 \quad v_3\}^T$$

$$\boldsymbol{U}_u = \{v_1 \quad v_6 \quad \phi_1 \quad \phi_2 \quad \phi_3 \quad \phi_4 \quad \phi_5 \quad \phi_6\}^T$$

$$\boldsymbol{F}_b = \{-K_{v1}v_1 \quad -K_{\phi 1}\phi_1 \quad -K_{v2}v_6 \quad -K_{\phi 2}\phi_6\}^T$$

$$\boldsymbol{F}_e = \{P \quad 0 \quad 0 \quad 0 \quad 0 \quad 0 \quad 0 \quad 0\}^T$$

$$\boldsymbol{A}_{\mathrm{bm}} = \begin{bmatrix} s^1_{13} & 0 & 0 & 0 \\ s^1_{23} & 0 & 0 & 0 \\ 0 & 0 & 0 & s^5_{31} \\ 0 & 0 & 0 & s^5_{41} \end{bmatrix}$$

$$\boldsymbol{A}_{\mathrm{bu}} = \begin{bmatrix} s^1_{11} & 0 & s^1_{12} & s^1_{14} & 0 & 0 & 0 & 0 \\ s^1_{21} & 0 & s^1_{22} & s^1_{24} & 0 & 0 & 0 & 0 \\ 0 & s^5_{33} & 0 & 0 & 0 & 0 & s^5_{32} & s^5_{34} \\ 0 & s^5_{43} & 0 & 0 & 0 & 0 & s^5_{42} & s^5_{44} \end{bmatrix}$$

$$\boldsymbol{A}_{\mathrm{em}} = \begin{bmatrix} s^1_{33} + s^2_{11} & s^2_{13} & 0 & 0 \\ s^1_{43} + s^2_{21} & s^2_{23} & 0 & 0 \\ s^2_{31} & s^2_{33} + s^3_{11} & s^3_{13} & 0 \\ s^2_{41} & s^2_{43} + s^3_{21} & s^3_{23} & 0 \\ 0 & s^3_{31} & s^3_{33} + s^4_{11} & s^4_{13} \\ 0 & s^3_{41} & s^3_{43} + s^4_{21} & s^4_{23} \\ 0 & 0 & s^4_{31} & s^4_{33} + s^5_{11} \\ 0 & 0 & s^4_{41} & s^4_{43} + s^5_{21} \end{bmatrix}$$

$$\boldsymbol{A}_{\text{eu}} =$$

$$\begin{bmatrix}
s_{31}^1 & 0 & s_{32}^1 & s_{34}^1 + s_{12}^2 & s_{14}^2 & 0 & 0 & 0 \\
0 & s_{42}^1 & s_{44}^1 + s_{22}^2 & s_{24}^2 & 0 & 0 & 0 & s_{41}^1 \\
0 & 0 & s_{32}^2 & s_{34}^2 + s_{12}^3 & s_{14}^3 & 0 & 0 & 0 \\
0 & 0 & s_{42}^2 & s_{44}^2 + s_{22}^3 & s_{24}^3 & 0 & 0 & 0 \\
0 & 0 & 0 & s_{32}^3 & s_{43}^3 + s_{12}^4 & s_{14}^4 & 0 & 0 \\
0 & 0 & 0 & s_{42}^3 & s_{44}^3 + s_{22}^4 & s_{24}^4 & 0 & 0 \\
s_{13}^5 & 0 & 0 & 0 & s_{32}^4 & s_{34}^4 + s_{12}^5 & s_{14}^5 & 0 \\
s_{23}^5 & 0 & 0 & 0 & s_{42}^4 & s_{44}^4 + s_{22}^5 & s_{24}^5 & 0
\end{bmatrix} \tag{23}$$

Equation (22) can be rewritten in terms of the nodal inertance vector $\boldsymbol{D}$, instead of the nodal displacement vector $\boldsymbol{U}$, as

$$\begin{bmatrix} \boldsymbol{A}_{\text{bm}} & \boldsymbol{A}_{\text{bu}} \\ \boldsymbol{A}_{\text{em}} & \boldsymbol{A}_{\text{eu}} \end{bmatrix} \begin{Bmatrix} \boldsymbol{D}_m \\ \boldsymbol{D}_u \end{Bmatrix} = \begin{Bmatrix} \boldsymbol{f}_b \\ \boldsymbol{f}_e \end{Bmatrix} \tag{24}$$

where

$$\begin{aligned}
\boldsymbol{D}_m &= (-\omega^2/P)\boldsymbol{d}_m = \{a_2 \quad a_3 \quad a_4 \quad a_5\}^T \\
\boldsymbol{D}_u &= (-\omega^2/P)\boldsymbol{d}_u = \{a_1 \quad a_6 \quad \alpha_1 \quad \alpha_2 \quad \alpha_3 \quad \alpha_4 \quad \alpha_5 \quad \alpha_6\}^T \\
\boldsymbol{f}_b &= (-\omega^2/P)\boldsymbol{F}_b = \{-K_{v1}a_1 \quad -K_{\phi 1}\alpha_1 \quad -K_{v2}a_6 \quad -K_{\phi 2}\alpha_6\}^T \\
\boldsymbol{f}_e &= (-\omega^2/P)\boldsymbol{F}_e = \{-\omega^2 \quad 0 \quad 0 \quad 0 \quad 0 \quad 0 \quad 0 \quad 0\}^T
\end{aligned} \tag{25}$$

From Eq. (25c) the effective boundary spring constants can be obtained in terms of unknown boundary forces as

$$\begin{Bmatrix} K_{v1} \\ K_{\phi 1} \\ K_{v2} \\ K_{\phi 2} \end{Bmatrix} = \begin{bmatrix} 1/a_1 & 0 & 0 & 0 \\ 0 & 1/\alpha_1 & 0 & 0 \\ 0 & 0 & 1/a_6 & 0 \\ 0 & 0 & 0 & 1/\alpha_6 \end{bmatrix} \boldsymbol{f}_b \tag{26}$$

The unknown boundary forces vector $\boldsymbol{f}_b$ can be obtained in terms of only $\boldsymbol{D}_m$ and $\boldsymbol{f}_e$ from the same formula as given in Eq. (19). The effective boundary spring constants are then readily determined by substituting $\boldsymbol{f}_b$ into Eq. (26).

IV. Experiment, Analysis, and Discussion

A. Experiments

Experiments are conducted for two aluminum beams with different boundary conditions: a one-end-supported (cantilever-type) beam and a two-end-supported beam. The experimental setup for the cantilevered beam is shown in Fig. 5. The lengths are 0.5 m for the one-end-supported beam and 0.65 m for the two-end-supported beam. For both beams the width and thickness are 0.03 and 0.05 m, respectively.

The vise is carefully designed so as to minimize its effects on the dynamic characteristics of beam specimen within the frequency range of concern, i.e., 1 kHz. Impact hammer is used to apply a wide exciting spectrum. The impact point and the response measurement point are chosen not to be near the node points (points of zero

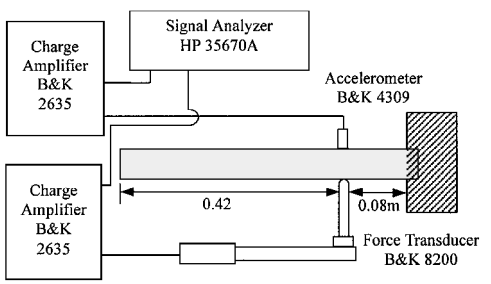

Fig. 5 Experimental apparatus for the one-end-supported beam.

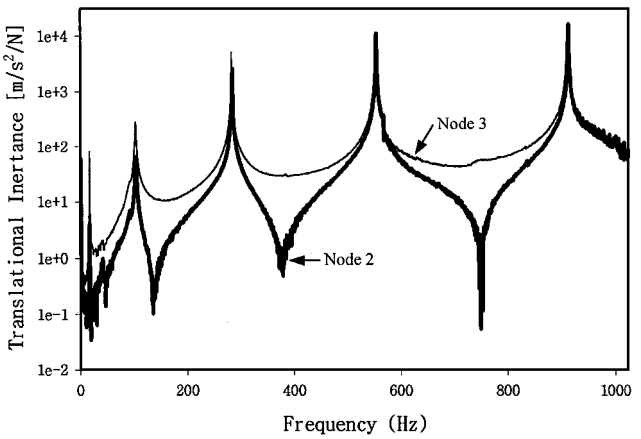

Fig. 6 Measured transverse inertances at nodes 2 and 3 of the one-end-supported beam.

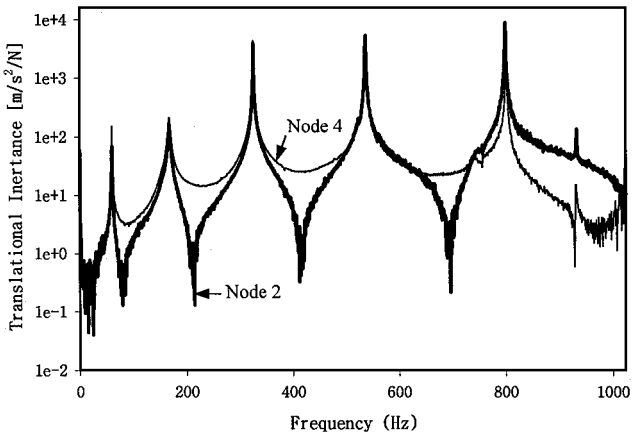

Fig. 7 Measured transverse inertances at nodes 2 and 4 of the two-end-supported beam.

motion). The coherence functions are carefully reviewed to select the final response measurement points. In the signal analyzer the sampling time is setup as 2 s. Although the vibration test for the simple beams is not a hard task in these days, the same test has been repeated several times, and the best test results are chosen for use.

Measured exciting forces and accelerations are transformed into the frequency domain by using the FFT algorithm of MATLAB, and the results are used to compute the nodal transverse and rotational inertances defined in Eqs. (16) and (25). Figure 6 shows the nodal transverse inertances measured at nodes 2 and 3 of the cantilevered beam, and Fig. 7 shows the nodal transverse inertances measured at nodes 2 and 4 of the two-end-supported beam.

B. Analysis and Discussion

The frequency range of concern in this paper is about 1 kHz for both theoretical analysis and experiments. The lowest natural frequency of axial modes is about 2580 Hz for the one-end-supported beam and about 5160 Hz for the two-end-supported beam. Thus the effects of axial modes are expected to be negligible. Thus, they are neglected in the preceding theoretical formulation and also in the following theoretical predictions.

Using the measured nodal transverse inertances as shown in Figs. 6 and 7, the unmeasured nodal inertances and the unmeasured effective boundary spring constants are computed by using the MATLAB program ID-BC developed in this study. Figures 8 and 9 illustrate the calculated unmeasured nodal inertances at node 1 of the one-end-supported beam and at nodes 1 and 6 of the two-end-supported beam, respectively.

The calculated effective boundary spring constants are shown in Fig. 10 for one-end-supported beam and in Fig. 11 for the two-end-supported beam, respectively. They are all frequency-dependent. The frequency-dependent spectral element matrix (also named as

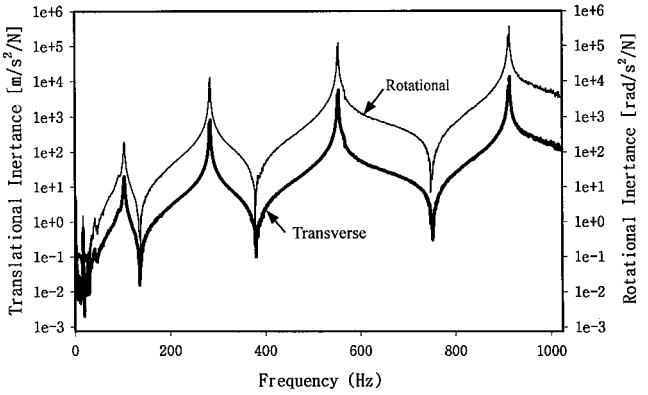

Fig. 8 Predicted rotational and transverse inertances at node 1 of the one-end-supported beam.

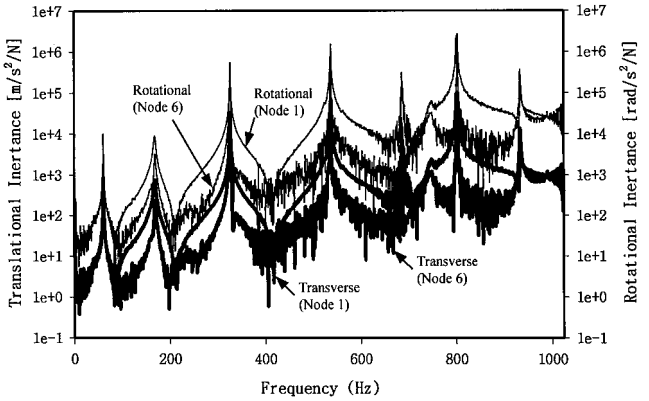

Fig. 9 Predicted rotational and transverse inertances at node 1 and 6 of the two-end-supported beam.

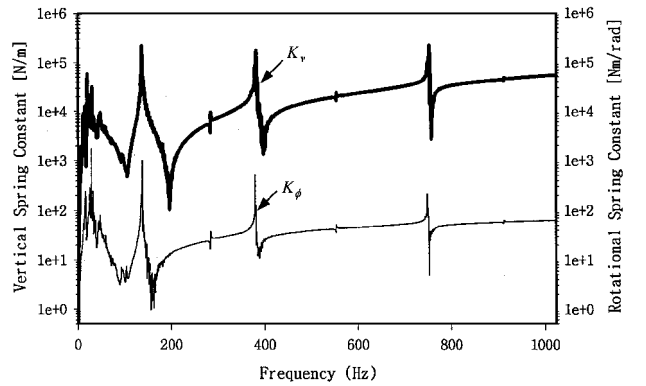

Fig. 10 Effective boundary spring constants for the one-end-supported beam.

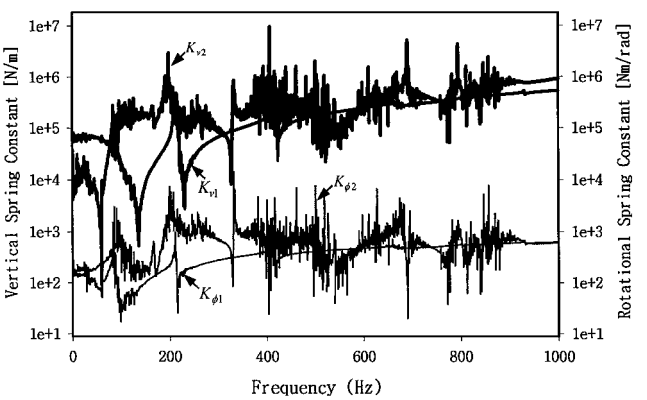

Fig. 11 Effective boundary spring constants for the two-end-supported beam.

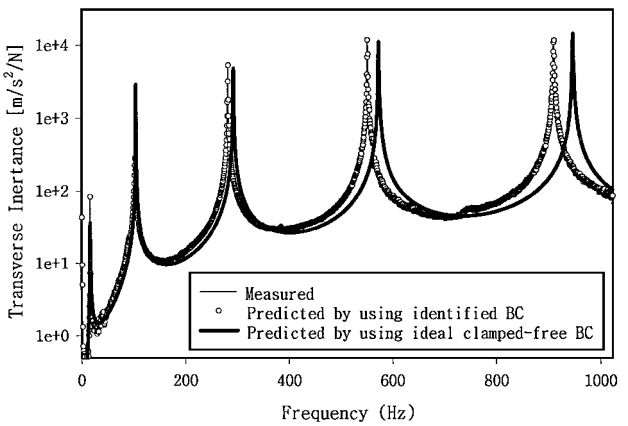

Fig. 12 Comparison of the measured and predicted transverse inertances at node 3 of the one-end-supported beam.

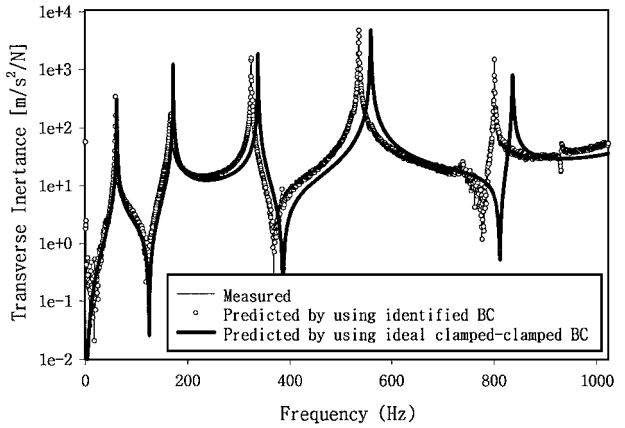

Fig. 13 Comparison of the measured and predicted transverse inertances at node 4 of the two-end-supported beam.

the exact dynamic stiffness matrix) implies that the elastic stiffness cannot be assumed to be constant (i.e., frequency independent) in dynamics any more, although it is very customary to assume the elastic stiffness constant in statics. In a very similar sense it seems to be natural that the effective boundary springs are also frequency-dependent in dynamics. To compute the natural frequencies of each beam, substitute the identified frequency-dependent spring constants into Eq. (12) or Eq. (20) and find the roots of the determinant of corresponding global spectral matrix $\boldsymbol{S}$. The theoretically predicted natural frequencies can be observed from Figs. 12 and 13.

To investigate the effects of the nonideality of beam boundary on the beam vibration characteristics, two theoretically predicted results are compared with the measured results: one is predicted by using the identified boundary conditions (i.e., effective boundary spring constants) and the other one is by using the ideal boundary conditions. For all predictions SEM is used. As the ideal boundary conditions, the clamped–free boundary conditions are used for the one-end-supported beam, whereas the clamped–clamped boundary conditions are used for the both-end-supported beam.

Figures 12 and 13 show the comparison of the theoretically predicted and measured inertances (FRF). When the identified boundary conditions are used for theoretical predictions, the predicted inertances are found to be almost identical to the measured results because the nonideal (or unknown) boundary conditions are so determined in frequency domain as to match the measured data exactly. However, when idealized boundary conditions are used instead, the predicted inertances are found to deviate significantly from the measurements as the frequency increases. This certainly implies the importance of the accurate identification of nonideal boundary conditions.

As already mentioned, the nonideal (or unknown) boundary conditions are so determined in frequency domain as to match the measured data exactly, thus the theoretically predicted inertances are

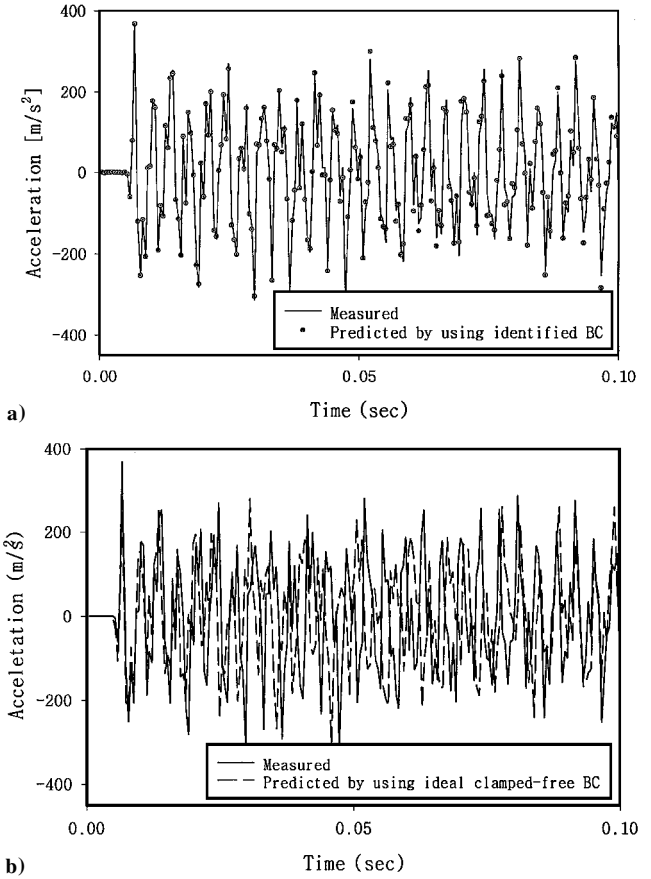

Fig. 14 Comparison of the measured and predicted accelerations at node 3 of the one-end-supported beam.

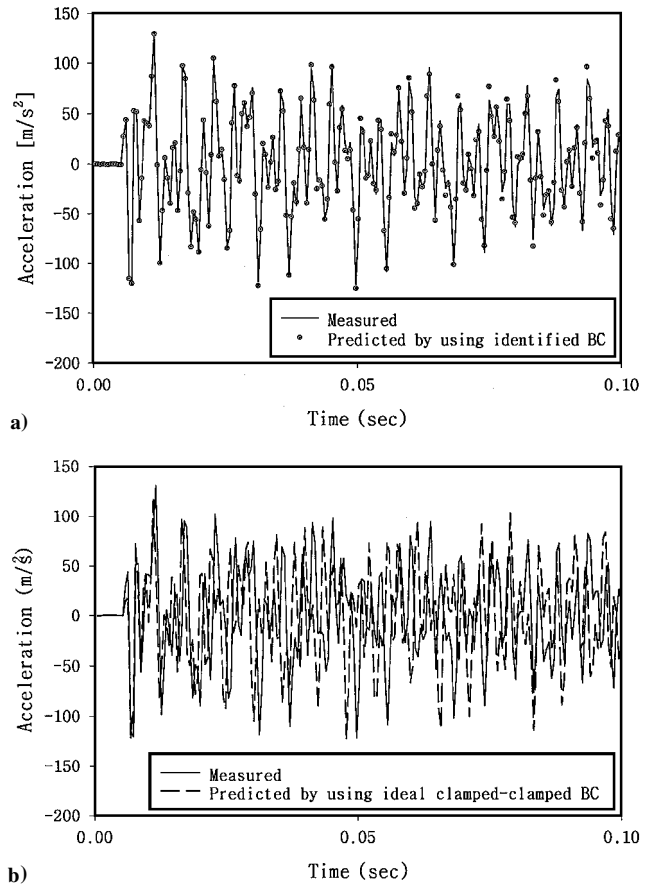

Fig. 15 Comparison of the measured and predicted accelerations at node 4 of the two-end-supported beam.

identical to the measured results. In fact, the uncertainties (or errors) involved in the mathematical beam model and the possible energy flow (or damping) through the boundaries are all smeared into the effective boundary spring constants. Thus, to identify pure (or exact) boundary conditions, one has to remove all uncertainties that may contaminate the pure boundary conditions. Thus, the more accurate beam model (e.g., Timoshenko beam model instead of Bernoulli–Euler beam model) will be better to achieve more accurate identification of boundary conditions. This paper can be readily extended to use more accurate beam models, and it is in due course.

In Figs. 14 and 15 the measured accelerations are compared with the theoretically predicted time responses. Figures 14a and 15a show the accelerations predicted by using identified boundary conditions that are quite close to the measured data. However, a small discrepancy is observed with the lapse of time. Because the predicted accelerations are obtained from exactly predicted FRF by using inverse FFT algorithm, the small discrepancy observed with the lapse of time seems to occur because of the inherent numerical errors and also because of the miss of high-frequency spectral components from time-domain solutions. The high-frequency spectral components beyond Nyquist frequency cannot be included in the time-domain solutions because the FFT and IFFT algorithms are used in the spectral element analysis procedure. Thus, improved theoretical predictions may be achieved by further increasing the Nyquist frequency.

As expected, in contrast to the predictions based on identified boundary conditions, Figs. 14b and 15b show that there exists quite a large discrepancy between accelerations predicted by using ideal boundary conditions and measuring results. In this case the discrepancy is caused by many sources such as the inaccurate boundary conditions, the effects of transverse shear, and rotary inertia neglected in the present Bernoulli–Euler beam model, and so forth.

V. Conclusions

This paper introduces a method to determine the nonideal boundary conditions of beam structures by using the spectral element method. The nonideal boundary is represented as the effective boundary springs, and they are determined from measured FRF. The present approach of boundary conditions identification is verified by comparing the measured dynamic responses with the analytical results predicted by using the identified boundary conditions. In general, it is found that the identified boundary conditions identified by the present approach give very accurate dynamic responses of a beam structure.

Acknowledgment

This study is supported by the 1999 Inha University Research Fund.

References

[1]Fabunmi, J. A., "Spectral Basis Theory for the Identification of Structural Dynamic Systems," *AIAA Journal*, Vol. 8, No. 6, 1988, pp. 726–732.

[2]Chen, S. Y., Ju., M. S., and Tsuei, Y. G., "Estimation of Mass, Stiffness, and Damping Matrices from Frequency Response Functions," *Journal of Vibration and Acoustics*, Vol. 118, Jan. 1996, pp. 78–82.

[3]Zimmerman, D. C., Smith, S. W., Kim, H. M., and Bartkowicz, T. J., "An Experimental Study of Structural Health Monitoring Using Incomplete Measurements," *Journal of Vibration and Acoustics*, Vol. 118, Oct. 1996, pp. 543–550.

[4]Wang, F., and Chen, S., "A Method to Determine the Boundary Condition of the Finite Element Model of a Slender Beam Using Measured Modal Parameters," *Journal of Vibration and Acoustics*, Vol. 118, July 1996, pp. 474–478.

[5]Doyle, J. F., *Wave Propagation in Structure: Spectral Analysis Using Fast Discrete Fourier Transforms*, Springer–Verlag, New York, 1997.

[6]Lee, J., and Lee, U., "Spectral Element Analysis of the Structure Under Dynamic Distributed Loads," *Proceedings of the AIAA/ASME/ASCE/AHS/ASC 37th Structures, Structural Dynamics, and Materials Conference*, Pt. 3, AIAA, Reston, VA, 1996, pp. 1605–1614.

[7]Lee, U., and Lee, J., "Dynamic Analysis of One- and Two-Dimensional Structures Using Spectral Element Methods," *Proceedings of the 6th International Conference on Recent Advances in Structural Dynamics*, Vol. 1, edited by N. S. Ferguson, H. F. Wolfe, and C. Mei, Inst. of Sound and Vibration Research, Univ. of Southampton, Southampton, England, U.K., 1997, pp. 263–277.

[8]Lee, J., "Structural Dynamic Analysis Using Spectral Element Method," Ph.D. Dissertation, Dept. of Mechanical Engineering, Inha Univ., Inchon, Republic of Korea, Aug. 1997.

[9]Lee, U., "Equivalent Continuum Representation of Lattice Beams: Spectral Element Approach," *Engineering Structures*, Vol. 20, No. 7, 1998, pp. 587–592.

[10]Lee, U., and Lee, J., "Spectral Element Method for Levy-Type Plates Subject to Dynamic Loads," *Journal of Engineering Mechanics*, Vol. 125, No. 2, 1999, pp. 243–247.

[11]Doyle, J. F., "A Spectrally Formulated Finite Element for Longitudinal Wave Propagation," *International Journal of Analytical and Experimental Modal Analysis*, Vol. 3, No. 1, 1988, pp. 1–10.

[12]Rizzy, S. A., and Doyle, J. F., "A Spectral Element Approach to Wave Motion in Layered Solids," *Journal of Vibration and Acoustics*, Vol. 114, Oct. 1992, pp. 569–577.

[13]Brigham, E. O., *The Fast Fourier Transform and Its Applications*, Prentice–Hall, Upper Saddle River, NJ, 1988.

[14]Ewins, D. J., *Modal Testing: Theory and Practice*, Research Studies Press, Letchworth, Hertfordshire, England, U.K., 1986.

G. A Kardomateas
Associate Editor